ACS OMEGA

http://pubs.acs.org/journal/acsodf

Article

Tuning the Dielectric Constant and Surface Engineering of a $BaTiO_3$/Porous PDMS Composite Film for Enhanced Triboelectric Nanogenerator Output Performance

Doldet Tantraviwat,* Mutita Ngamyingyoud, Witsaroot Sripumkhai, Pattaraluck Pattamang, Gobwute Rujijanagul, and Burapat Inceesungvorn

Cite This: *ACS Omega* 2021, 6, 29765−29773

Read Online

ACCESS | Metrics & More | Article Recommendations | Supporting Information

ABSTRACT: In this work, synergistic effects derived from surface engineering and dielectric property tuning were exploited to enhance the output performance of a triboelectric nanogenerator (TENG) based on an inorganic/porous PDMS composite in a contact−separation mode. $BaTiO_3$ (BT)/porous PDMS films with different BT weight ratios were fabricated and evaluated for triboelectric nanogenerator (TENG) application. Maximum output signals of ca. 2500 V, 150 μA, and a power density of 1.2 W m^{-2} are achieved from the TENG containing 7 wt % BT, which is the best compromise in terms of surface roughness, dielectric constant, and surface contact area as evidenced by SEM and AFM studies. These electrical signals are 2 times higher than those observed for the TENG without BT. The 7BT/porous PDMS-based TENG also shows high stability without a significant loss of output voltage for at least 24 000 cycles. With this optimized TENG, more than 350 LEDs are lit up and a wireless transmitter is operated within 9 s. This work not only shows the promoting effects from porous surfaces and an optimized dielectric constant but also offers a rapid and template/waste-free fabrication process for porous PDMS composite films toward large-scale production.

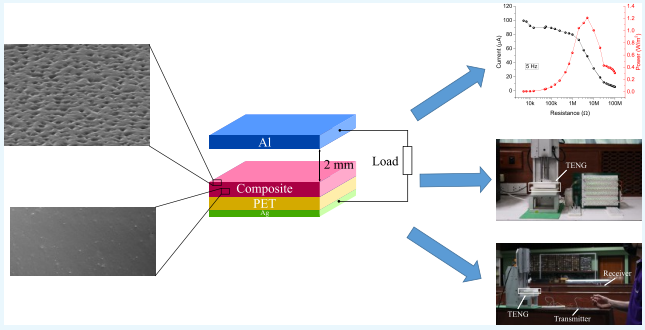

1. INTRODUCTION

Small, portable, and wearable low-powered electronics such as smart watches and health monitoring sensors have increasingly been integrated into our everyday lives. These devices, however, are mostly powered by batteries that have caused unfavorable environmental consequences and limited further applications as flexible, self-sustainable, and biocompatible electronic systems.[1,2] Therefore, it is desirable to integrate flexible, environmentally friendly, and renewable energy harvesters into these electronics not only to alleviate environmental problems associated with batteries but also to realize self-powered systems with more flexibility to mechanical deformations under real working conditions. For these purposes, a triboelectric nanogenerator (TENG) has emerged as a promising sustainable energy harvesting technology that transforms wasted mechanical energies from the surrounding environment into electricity via the coupling mechanism of triboelectrification and electrostatic induction.[3−8] With TENG technology, real-time monitoring and self-powered electronics for modern healthcare diagnostics and delicate mechanical/chemical sensing have successfully been demonstrated.[9−13]

Poly(dimethylsiloxane) (PDMS) is one of the most negative tribomaterials commonly used in TENG because of its flexibility, high electronegativity, nontoxicity, and biocompatibility. To enhance PDMS-based TENG electrical performance, various structures and patterns such as micro/nanoporous and sponge-like structures are created to increase the porosity, surface roughness, and hence effective contact area of the PDMS film.[14−17] Additionally, incorporating high dielectric inorganic materials into a PDMS matrix could promote the relative permittivity and charge density of tribomaterials, which further boost the PDMS-based TENG electrical output.[18−22] Therefore, increasing both surface porosity and dielectric constant of the tribomaterials is expected to substantially boost the electrical performance of PDMS composite-based TENGs.[2,23] To fabricate highly porous PDMS composites, sacrificial agents or excess organic solvents are often required to achieve high porosity and well-dispersed inorganic particles.[17,20,24,25] Consequently, additional steps to eliminate sacrificial templates and solvents are inevitable. For example, microwave irradiation was employed for the fabrication of sponge-type PDMS, the pore size of which depends on the boiling point of the sacrificial

Received: August 6, 2021
Accepted: October 15, 2021
Published: October 29, 2021

ACS Publications

© 2021 The Authors. Published by American Chemical Society

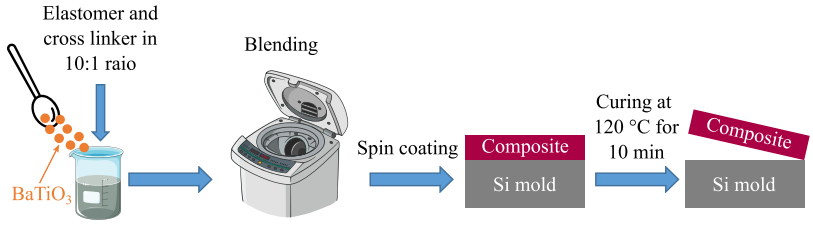

Figure 1. Schematic diagram for the fabrication process of the BT/porous PDMS composite layer.

solvent.[24] NaCl and Na_2CO_3 were used as sacrificial templates for porous PDMS composite films. A porous structure was then obtained after immersing the template/PDMS film in excess water under constant stirring[17] or bath sonication.[25] A polystyrene sphere (PS) was used to fabricate a PDMS inverse opal-structured film, from which the sphere was later removed by soaking the PS-embedded PDMS film in acetone for at least 24 h to ensure complete removal.[16] These fabrication methods not only generate chemical wastes but also make the process more time-consuming and cause inefficient chemical usage. Therefore, the development of rapid and environmentally friendly fabrication processes is necessary.

Encouraged by the literature above, a combined approach of surface engineering and an increasing dielectric constant was adopted to enhance the output performance of an inorganic/PDMS composite-based TENG using a fast and waste-free fabrication process developed in this work. To the best of our knowledge, there have been no attempts to explore the possibility of making porous PDMS-based composites without using sacrificial agents or organic solvents. By taking the advantage of centrifugal and shearing forces for fabricating PDMS composites and silicon molds for surface patterning, a fast, solventless, and template-free fabrication process was achieved. The process employed herein can fabricate each porous PDMS composite film within 15 min and thus is favorable to large-scale production. The results revealed that open-circuit voltage (V_{OC}) and short-circuit current (I_{SC}) of the TENG with a composite film were almost twofold compared to those of the TENG with bare porous PDMS. The application of the BT/porous PDMS-based TENG as an energy supply for LEDs and wireless transmitters as well as its durability was also well demonstrated.

2. RESULTS AND DISCUSSION

$BaTiO_3$ (BT) was chosen as a model inorganic dielectric due to its high relative permittivity. As illustrated in Figure 1, the fabrication process of a BT/porous PDMS composite layer began by mixing a PDMS elastomer and a cross linker (Sylgard 184, Tow Corning) in a 10:1 weight ratio. BT powders (an average particle size of <3 μm, Sigma-Aldrich) in different weight percentages (0, 2.5, 5, 7, 9, 13, 17, 20, and 23 wt %) were then added to the PDMS mixture. The samples were named *x*BT/porous PDMS, where *x* is the BT weight percentage. The resulting mixture was blended using a planetary centrifugal mixer (ARE-310, Thinky Co.) at a revolution speed of 1800 rpm for 90 s and then at 1500 rpm for 40 s. A surface patterning technique modified by our previous work[26] was used to create a porous PDMS surface utilizing a nanograss silicon (Si) mold. After the nanograss Si mold was treated with hexamethyldisilazane (HMDS, J.T.Baker), the blended BT/PDMS mixture was subsequently cast on the mold using spin coating at 250 rpm for 30 s and then at 350 rpm for another 30 s. The composite film was thermally cured at 120 °C for 10 min and finally peeled off. The average film thickness was ca. 130 μm. No solvent or sacrificial templates were required in the process.

Top-view SEM images of bare PDMS and its composite films with 7, 9, and 17 wt % BT are displayed in Figure 2a–d,

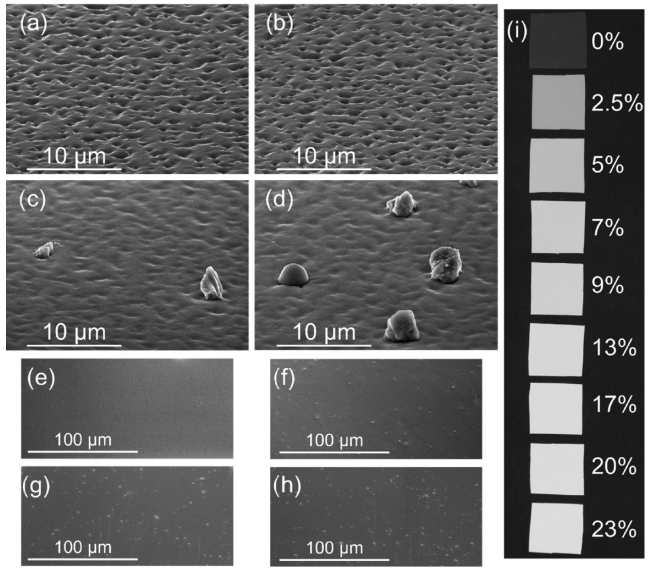

Figure 2. SEM images showing the surface (a–d) and cross section (e–h) of the composite films: 0BT/porous PDMS (a, e), 7BT/porous PDMS (b, f), 9BT/porous PDMS (c, g), and 17BT/porous PDMS (d, h). Photographs of *x*BT/porous PDMS composite films (i) fabricated with different BT amounts.

respectively. A rough surface with a highly porous structure is visibly observed for bare PDMS (Figure 2a). The film can retain its porous structure with the increase of the BT amount from 2.5 to 7 wt % (Figures S1a,b and 2b), indicating successful pattern transfer for the inorganic/porous PDMS composite film. By increasing the BT content further to 9 and 17 wt % (Figure 2c,d), protruded particles can easily be found on the PDMS surface. Moreover, the films also lose their porous feature, as shallow pore depth can be clearly observed. This is probably because blended mixtures with high particle contents tend to have higher viscosity, resulting in the lower fidelity of pattern transfer[27,28] and the greater probability of particles emerged from the polymer surface.[17] Cross-sectional SEM images of bare porous PDMS and *x*BT/porous PDMS films (Figures 2e–h and S2) reveal well-dispersed BT particles in films containing BT up to 17 wt %; however, the agglomeration of particles is easily spotted on increasing the BT content further. Digital images of all *x*BT/porous PDMS films (Figure 2i) show that transparent PDMS changes to homogeneous opaque white when BT particles were introduced. Here, the blending step is important to achieve the high dispersibility of BT particles and complete

https://doi.org/10.1021/acsomega.1c04222
ACS Omega 2021, 6, 29765−29773

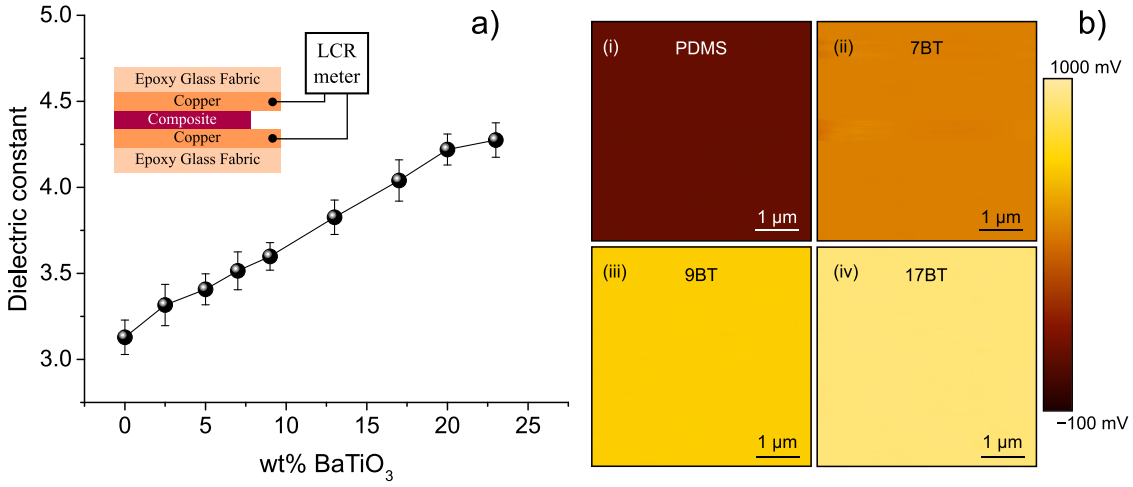

Figure 3. (a) Dielectric constant of the composite film as a function of $BaTiO_3$ weight percentage. The inset illustrates an experimental setup for parallel plate capacitor measurement. (b) KFPM measurement showing different surface charge potentials of (i) bare PDMS and composite films with (ii) 7 wt %, (iii) 9 wt %, and (iv) 17 wt % of BT.

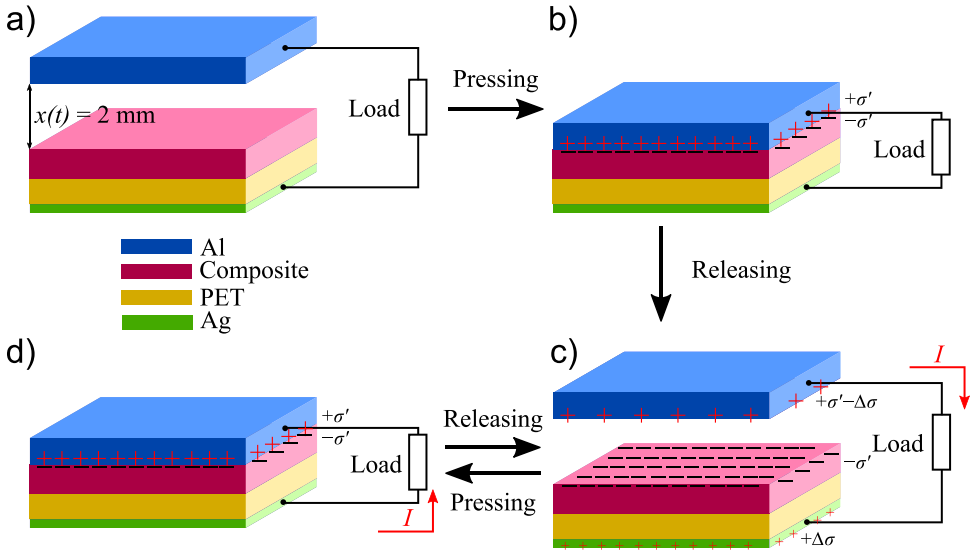

Figure 4. (a–d) Charge generation mechanism of the porous PDMS composite-based TENG under an external force.

deaeration. Spiral vortical flow within the container generated by a combination of shearing and centrifugal forces promotes mixing and degassing at the same time.[29,30] Each BT/porous PDMS composite film can successfully be fabricated in less than 15 min without any additional solvent/template elimination steps, which is favorable to large-scale fabrication.

Triboelectric charge transfer occurs during contact between the triboelectric materials, and it is this transferred charge density that determines the output performance of TENGs. According to previous reports,[31,32] the dielectric constant of the triboelectric material is a critical factor boosting the maximum charge density (σ') expressed as follows[32]

$$\sigma' = \frac{\sigma_0 \cdot x(t)}{x(t) + d_{\mathrm{PDMS}}/\varepsilon_{\mathrm{PDMS}}} \tag{1}$$

where σ_0 is the triboelectric charge density at the equilibrium state, $x(t)$ is the gap distance (2 mm in this study), and d_{PDMS} and $\varepsilon_{\mathrm{PDMS}}$ are the thickness and dielectric constant of the PDMS-based film. Therefore, increasing the dielectric constant would improve the maximum charge density and TENG output performance. The dielectric properties of triboelectric materials constituted in the TENG device have shown a strong influence on capacitive characteristics and corresponding TENG electrical output performance.[17,21,33] To measure the capacitance of the obtained *x*BT/porous PDMS composite, the film was sandwiched between two single-sided copper boards to form a parallel plate capacitor (the inset of Figure 3a), and its dielectric constant was determined from the following equation

$$C = \frac{A \cdot \varepsilon_0 \cdot \varepsilon_r}{d_{\mathrm{composite}}} \tag{2}$$

where C, ε_0, ε_r, A, and $d_{\mathrm{composite}}$ are the measured capacitance, vacuum permittivity of free space (8.85×10^{12} F m^{-1}), relative permittivity (also called dielectric constant), area, and thickness of the composite material, respectively. From Figure 3a, the dielectric constant of bare porous PDMS is ca. 3.13, which is consistent with other studies.[34,35] As expected, the dielectric constant increases almost linearly with the increase of the BT weight ratio and reaches a maximum value of ca. 4.27 for the 23BT/porous PDMS film. A similar trend was found in previous

https://doi.org/10.1021/acsomega.1c04222
ACS Omega 2021, 6, 29765−29773

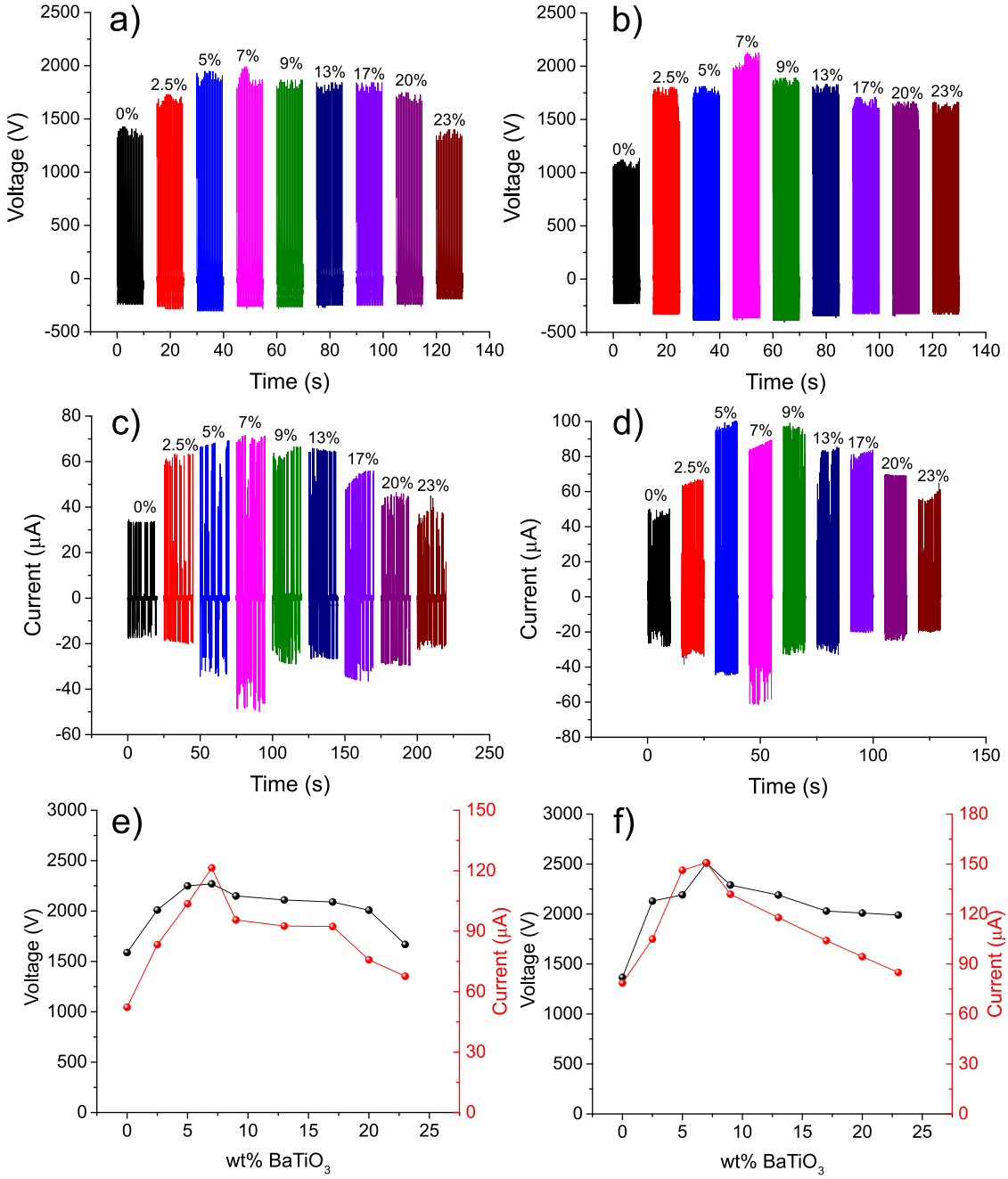

Figure 5. V_{OC} (a, b), I_{SC} (c, d), and their peak-to-peak value (e, f) of the *x*BT/porous PDMS-based TENGs as a function of BT content at pressing frequencies of 2 Hz (a, c, e) and 5 Hz (b, d, f).

reports, although with different dielectric constant values,[17,21,36] which is probably due to diverse degrees of particle distribution and agglomeration, compromising the homogeneity of the composite films. Because the surface potential of materials can also affect TENG output performance,[37] the surface potential of the obtained composite films was therefore measured by the KPFM technique. From Figure 3b, the average surface potentials for PDMS composite films with BT contents of 0, 7, 9, and 17 wt % are 85.77, 495.63, 710.06, and 926.42 mV, respectively. Clearly, increasing the BT particles also improves the surface potential of the composite films. Since the TENG can be simply modeled as a parallel plate capacitor,[22,32,38,39] such enhanced dielectric constant and increased surface potential achieved from the composite film would boost triboelectric charge density and improve the output performance of the TENG in harvesting mechanical energy.

Figure 4 presents the working mechanism of the *x*BT/porous PDMS-based TENG in a contact−separation mode by applying a periodic vertical force. The TENG comprises an aluminum sheet and an *x*BT/porous PDMS film as positive and negative triboelectric layers with an interlayer distance of 2 mm. As the composite-based TENGs are fabricated without a spacer, full contact between aluminum and composite films is expected. In the beginning, no charge is initially developed, as the two triboelectric layers are not in contact. As the aluminum film is pressed to come in contact with the composite film, triboelectrification occurs and surface charges with an opposite sign are generated between them. During this step, electron transfer

https://doi.org/10.1021/acsomega.1c04222
ACS Omega 2021, 6, 29765−29773

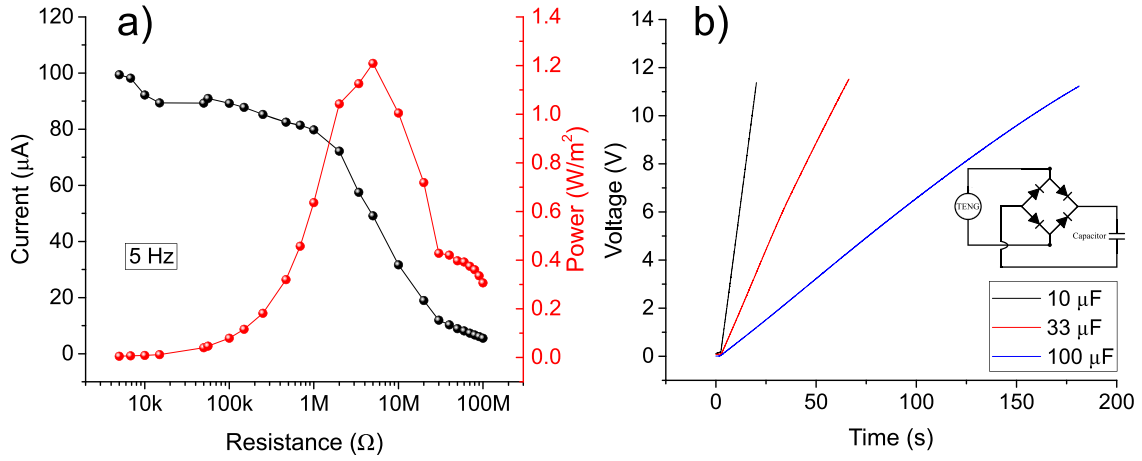

Figure 6. (a) Maximum output current and power as a function of external load resistance and (b) the charging ability of the 7BT/porous PDMS-based TENG at 5 Hz.

due to the electron affinity difference is generally considered as the main source of triboelectrification in metal−polymer TENGs.[17,40] However, contributions from ion transfer and material transfer mechanisms to contact electrification are also possible.[41] Since our electrical characterization was performed under the same relative humidity range (50−60%), the effect of ion transfer on all samples is relatively similar. A possible contribution from the material transfer mechanism is supported by the XPS results, as shown in Figure S3 and Table S1, from which an increase in Si 2p concentration is clearly observed on the surface of aluminum tape upon coming in contact with the PDMS composite film. As a result of these mechanisms, the composite layer by gaining electrons becomes negatively charged ($-\sigma'$), whereas the aluminum film by losing electrons becomes positively charged ($+\sigma'$). When the aluminum film is separated from the bottom structure, its positive charges attract electrons ($-\Delta\sigma$) from a bottom electrode (silver) through an external circuit until an equilibrium state, called the open-circuit voltage (V_{OC}) condition, is established (Figure 4c). At this moment, V_{OC} can be determined as follows[33]

$$V_{OC} = \frac{\sigma' \cdot x(t)}{\varepsilon_0} \tag{3}$$

Equation 3 indicates a direct relation between V_{OC} and σ', which is strongly influenced by the capacitance of the TENG configured in the contact−separation mode and the effective surface area.[42] Once the aluminum film comes again in contact with the composite layer, electrons flow from the aluminum film back to the silver electrode. An opposite current is therefore observed. At this point, $x(t)$ reduces to zero, leading to zero voltage potential according to eq 3. This is known as the short-circuit condition (I_{SC}), which is given by[33]

$$I_{SC} = \frac{A \cdot \sigma' \cdot d_{composite} \cdot v(t)}{(d_{composite} + x(t))^2} \tag{4}$$

where $v(t)$ is the velocity of contact−separation movement. It can be clearly seen from eqs 3 and 4 that both V_{OC} and I_{SC} are directly proportional to σ', which can be enhanced with the increase of the dielectric constant.

The xBT/porous PDMS-based TENGs were electrically characterized via a vertical contact−separation mode at different frequencies (1, 2, 4, and 5 Hz). Identical force and 2 mm distance between the aluminum and composite films were applied to all fabricated TENGs. As shown in Figure 5a−d, introducing BT particles into bare PDMS obviously promotes both V_{OC} and I_{SC} of the fabricated TENG. The output signals (Figure 5e,f) gradually enhance with the increase of the BT amount and reach their maximum values using the 7BT/porous PDMS composite. The composite layer with a higher dielectric constant possesses a higher surface charge density.[43] The intensity of the electrostatic induction, generated by the increased surface charges, is therefore stronger on both electrodes, which leads to the enhancement of V_{OC} and I_{SC}. Increasing the BT content further to 9 wt %, however, decreases the output performance. At 5 Hz (Figure 5f), the highest V_{OC} and I_{SC} observed for the TENG with the 7BT/porous PDMS film are ∼2500 V and ∼150 μA, respectively. These values are almost twice those measured using the bare porous PDMS film, which evidently indicates a successful enhancement of porous PDMS-based TENG efficiency by incorporating a high permittivity ceramic into the porous PDMS matrix. A similar trend, where the output performance first increases to its maximum and then decreases when a very high amount of $BaTiO_3$ was added, is also observed at frequencies of 1 and 4 Hz (Figure S4). Such behavior can be understood by considering two crucial factors that are the relative permittivity and surface contact area of the PDMS film. It is clear from Figure 3a,b that the dielectric constant and surface potential keep increasing with the increase of BT content; therefore, V_{OC} and I_{SC} should increase as well. However, V_{OC} and I_{SC} decrease with the increase of the BT amount to more than 7 wt %. As evidenced by SEM in Figure 2c, the composite film significantly loses its porosity, and the BT particles are clearly found on the PDMS surface when the BT content is higher than 7 wt %. Because PDMS is a superior tribomaterial than inorganic BT, a decrease in the PDMS surface area can result in a reduction of generated surface charge density (σ'). In addition, AFM investigation (Figure S5) also reveals that the average surface roughness (R_a) decreases with the increase of BT content. The R_a of the 7BT/porous composite is ca. 89.8 nm, while those of composite films with higher BT contents (9−23 wt %) are in the range of 72.7−65.7 nm. Previous studies[43−46] have shown that surface roughness is one of the most important factors influencing the output signals of TENGs. Lower surface roughness would have a smaller effective contact area and a low deformation level and therefore could generate less surface charge density during contacting and relaxing.[47−49] Therefore, such decreased V_{OC}

https://doi.org/10.1021/acsomega.1c04222
ACS Omega 2021, 6, 29765−29773

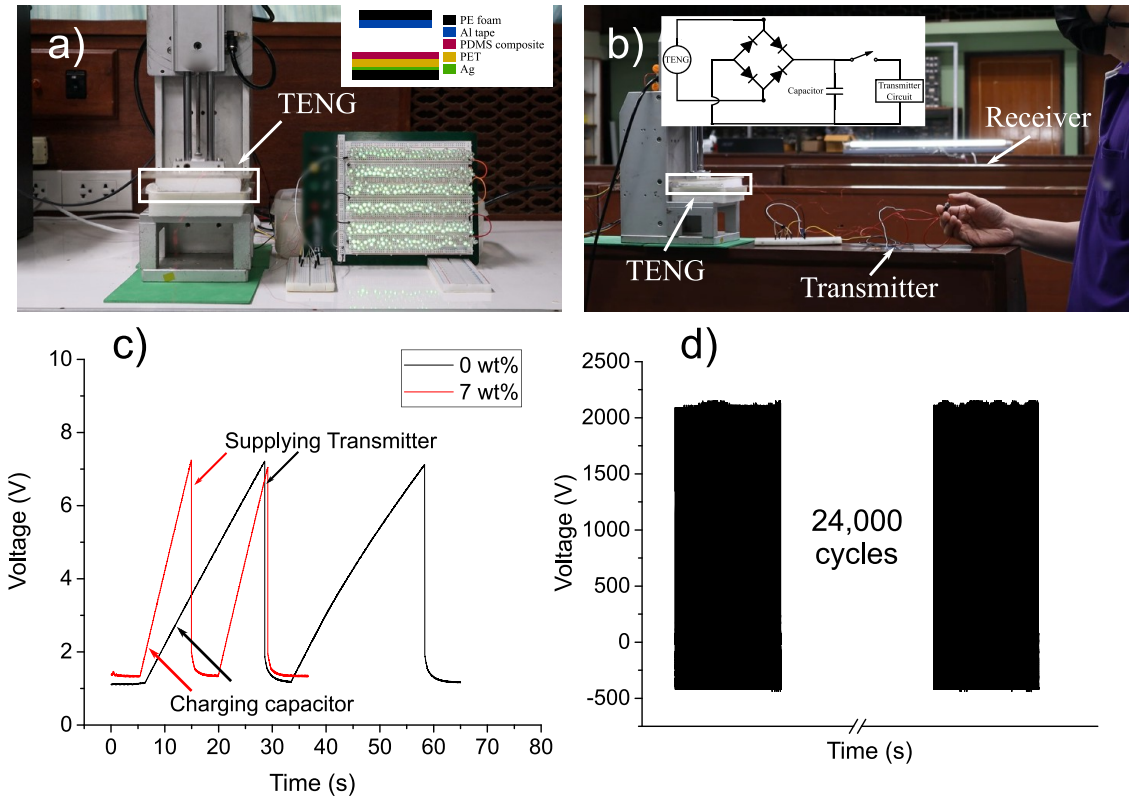

Figure 7. (a) Photograph of 372 green LEDs. The inset shows a schematic structural component of the TENG. (b) Wireless transmitter operated by the 7BT/porous PDMS-based TENG. (c) Comparison of capacitor voltage characteristics charged by porous PDMS-based TENGs with/without BT. (d) Stability and durability test of the PDMS composite-based TENG under a periodic compression of 5 Hz for >24 000 cycles.

and I_{SC} observed for composite films with high BT amounts are likely originated from a reduced surface contact area as supported by SEM and AFM analyses. The above characterization results indicate that the 7BT/porous composite film is the best compromise; therefore, the highest TENG output performance is observed. Our results correspond well with previous reports, although an optimum $BaTiO_3$ content may differ due to different TENG fabrication processes as well as diverse physical properties and homogeneity of $BaTiO_3$ particles in BT/PDMS composites.[24,36,46,50,51]

It can also be noticed from the results shown in Figures 5e,f and S4 that increasing the working frequency significantly affects I_{SC} but not V_{OC}, which is attributed to the fact that V_{OC} depends only on triboelectric charge density and the distance between two triboelectric materials (eq 3), which are constant for a certain TENG device. Since I_{SC} and the amount of transferred charges are closely related, the relationship between frequency and these two parameters for each TENG was further determined. The transferred charge was estimated from the measured peak current of TENGs using the equation $Q = \int i dt$, where i is the instantaneous current. The transferred charge density ($\Delta\sigma$) as a function of BT content is then plotted in Figure S6. The result shows that the maximum $\Delta\sigma$ is obtained from the 7BT/porous composite film, which is similar to those observed for V_{OC} and I_{SC}. A comparison between Figures 5e,f and S6 indicates that I_{SC} increases with increasing frequency, while the total amount of charges transferred remains almost the same. The results imply that the enhanced I_{SC} is mainly driven by the increased acceleration rate of contact−separation movement $v(t)$ (eq 4) rather than the number of transferred charges.

Because the 7BT/porous PDMS-based TENG provides the highest output performance among all TENGs studied here (Figure 5), this TENG was then chosen for further investigation. The maximum output power of the 7BT/porous PDMS-based TENG was determined by connecting the TENG to an external load with a resistance range of 5 kΩ−100 MΩ. As shown in Figure 6a, the current slightly decreases in a resistance range of 5 kΩ−2 MΩ since the charge transfer process, within this resistance range, is relatively similar to the short-circuit condition. It then drastically decreases with a resistive load of higher than 3 MΩ. The output current slowly approaches zero by further increasing the resistance beyond 20 MΩ. Based on these results, the maximum instantaneous power density of 1.21 W m^{-2} is achieved at a resistance value of 5 MΩ. The maximum power density of our device is in a similar range as the previous study,[24] in which a 3D porous PDMS/$BaTiO_3$ film was used. As the 3D porous network film generally has a large surface area, the comparable results here thus underline our porous composite-based TENG with boosting performance. The ability of the 7BT/porous PDMS-based TENG in charging different capacitors is also evaluated. As shown in Figure 6b, the composite-based TENG is used to charge 10, 33, and 100 μF capacitors under a periodic contact and separation mode at 5 Hz. After the TENG output is rectified, the 10, 33, and 100 μF capacitors are charged to 10 V in 18, 57, and 157 s, respectively.

The application of the composite-based TENG as a power source for low-powered electronics is also demonstrated. It can be used to drive at least 372 green LEDs connected in series to high brightness, even though the room is full of lights (Figure 7a and Video S1 in the Supporting Information). Furthermore, the electrical energy scavenged from the applied vertical force at 5

https://doi.org/10.1021/acsomega.1c04222
ACS Omega 2021, 6, 29765−29773

Hz can charge a 10 μF capacitor to 7 V within 9 s. This stored energy can then be successfully used to power a wireless transmitter circuit for sending a command to a receiver to turn on/off the light (Figure 7b and Video S2). The capacitor voltage characteristics of porous PDMS-based TENGs with and without BT are compared in Figure 7c. Evidently, the output performance of the PDMS composite-based TENG is far superior to that of the bare PDMS-based TENG, which needs almost 30 s to harvest enough energy to supply the transmitter. To evaluate the stability and durability of the 7BT/porous PDMS-based TENG, its electrical output voltage was measured for more than 40 min (at least 24 000 cycles). The output voltage is barely reduced, as presented in Figure 7d, implying the excellent stability and durability of the porous PDMS composite-based device fabricated in this work.

3. CONCLUSIONS

A BT/porous PDMS composite film was successfully fabricated using a fast, solventless, and template-free fabrication technique. The virtually linear relationship between the dielectric constant of the composite film and $BaTiO_3$ content is observed, suggesting successful incorporation between $BaTiO_3$ and PDMS using the developed technique. The BT/porous PDMS-based TENG shows superior output performance compared to the TENG with bare porous PDMS. Such enhanced performance could be attributed to the increase of surface charge density induced by the high dielectric constant and porous surface. The best output performance is accomplished from the PDMS composite-based TENG with 7 wt % $BaTiO_3$, producing voltage, current, and power density of ca. 2500 V, 150 μA, and 1.21 W m^{-2}, respectively. This optimized TENG also shows very high durability without a significant loss of its voltage for at least 24 000 cycles. The capability of such optimized TENG as a power source to drive commercial green LEDs and wireless transmitter circuits is successfully demonstrated. The simple, green, and scalable fabrication process for the porous PDMS composite film developed in this work would benefit large-scale production of the porous PDMS composite-based TENG and its practicality as a sustainable energy system in small electronic devices.

4. EXPERIMENT SECTION

4.1. Fabrication of the PDMS Composite-Based TENG.

Porous PDMS composite-based TENGs with different $BaTiO_3$ weight ratios in the vertical contact−separation mode were fabricated with an area of 10 × 10 cm^2. An expanded polyethylene form and an acrylic sheet were employed as supporting substrates. The top structure is constructed with aluminum tape attached to polyethylene foam. For the bottom part of the TENG, a PDMS composite film attached to a silver-coated PET film is fixed on the polyethylene foam using double-sided adhesive tape. The double-sided adhesive tape is used at all interfaces to prevent contact electrification that could possibly occur by interfacial friction.[52] The fabricated TENG was attached to a pushing tester, the top part of which can be moved up and down to adjust the distance between the top and bottom structures of the TENG. A gap distance of 2 mm was used throughout unless otherwise stated. The enameled conductor wires were then attached to the top and bottom electrodes by silver paste for measuring the output voltage and current signal.

4.2. Electrical and Material Characterization.

To measure the electrical outputs from TENGs, a custom-made pushing tester pneumatically operated was used to apply the external force on the TENGs. With solenoid valves fully opened for pressing and releasing actions during testing, the force applied on all TENGs should be the same. A digital oscilloscope (Agilent 2002A) with a 100:1 scope probe and a Keysight B2901A were employed to measure the open-circuit voltage (V_{OC}) and short-circuit current (I_{SC}), respectively. The capacitance value of the composite film was measured using a GW-Instek LCR-916 meter at three different frequencies (1, 10, and 100 kHz). The film surface morphology was investigated using a field emission scanning electron microscope (FE-SEM, Hitachi SU-8230). Surface roughness and Kelvin probe force microscopy measurements were performed using an atomic force microscope (AFM, Hitachi 5500M) with a rhodium-coated silicon tip (tip radius of 10 nm, force constant of 1.6 N m^{-1}, and resonance frequency of 28 kHz). The SEM and AFM measurements were performed on pristine samples. X-ray photoelectron spectroscopy (XPS) analysis was performed using a Kratos Axis Supra instrument.

■ ASSOCIATED CONTENT

Supporting Information

The Supporting Information is available free of charge at https://pubs.acs.org/doi/10.1021/acsomega.1c04222.

SEM images showing the surface of the composite film with different BT weight ratios: (a) 2.5 wt %, (b) 5 wt %, (c) 13 wt %, (d) 20 wt %, and (e) 23 wt %; SEM images showing the cross section of the composite film with different BT weight ratios: (a) 2.5 wt %, (b) 5 wt %, (c) 13 wt %, (d) 20 wt %, and (e) 23 wt %; XPS survey and Si 2p spectra of Al tapes before and after coming in contact with the PDMS composite film for a single and >24 000 press-release cycles; atomic composition determined from XPS measurement; V_{OC} (a, b), I_{SC} (c, d), and their peak-to-peak value (e, f) of the xBT/porous PDMS-based TENGs as a function of BT content at pressing frequencies of 1 Hz (a, c, e) and 4 Hz (b, d, f); AFM images showing surfaces of (a) bare PDMS and the composite films with different BT weight ratios: (b) 2.5 wt %, (c) 5 wt %, (d) 7 wt %, (e) 9 wt %, (f) 13 wt %, (g) 17 wt %, (h) 20 wt %, and (i) 23 wt %; and calculated transferred charge density as a function of BT content at different frequencies (PDF)

Application of the composite-based TENG as a power source for low-powered electronics (MP4)

Use of stored energy to power a wireless transmitter circuit for sending a command to a receiver to turn on/off the light (MP4)

■ AUTHOR INFORMATION

Corresponding Author

Doldet Tantraviwat − *Department of Electrical Engineering, Faculty of Engineering and Center of Excellence in Materials Science and Technology and Materials Science Research Center, Faculty of Science, Chiang Mai University, Chiang Mai 50200, Thailand;* orcid.org/0000-0001-7102-0883; Email: doldet.tantraviwat@cmu.ac.th

https://doi.org/10.1021/acsomega.1c04222
ACS Omega 2021, 6, 29765−29773

Authors

Mutita Ngamyingyoud − *Department of Electrical Engineering, Faculty of Engineering, Chiang Mai University, Chiang Mai 50200, Thailand*

Witsaroot Sripumkhai − *Thai Microelectronics Center (TMEC), National Electronics and Computer Technology Center (NECTEC), Chachoengsao 24000, Thailand*

Pattaraluck Pattamang − *Thai Microelectronics Center (TMEC), National Electronics and Computer Technology Center (NECTEC), Chachoengsao 24000, Thailand*

Gobwute Rujijanagul − *Center of Excellence in Materials Science and Technology and Materials Science Research Center, Faculty of Science, Chiang Mai University, Chiang Mai 50200, Thailand; Department of Physics and Materials Science, Faculty of Sciences, Chiang Mai University, Chiang Mai 50200, Thailand*

Burapat Inceesungvorn − *Center of Excellence in Materials Science and Technology and Materials Science Research Center, Faculty of Science, Chiang Mai University, Chiang Mai 50200, Thailand; Department of Chemistry, Faculty of Science, and Center of Excellence for Innovation in Chemistry (PERCH-CIC), Chiang Mai University, Chiang Mai 50200, Thailand*

Complete contact information is available at: https://pubs.acs.org/10.1021/acsomega.1c04222

Notes

The authors declare no competing financial interest.

■ ACKNOWLEDGMENTS

This work was supported by Center of Excellence in Materials Science and Technology; Chiang Mai University; Basic Research Fund, TSRI; Center of Excellence for Innovation in Chemistry (PERCH-CIC); and Ministry of Higher Education, Science, Research and Innovation.

■ REFERENCES

(1) Shi, Q.; He, T.; Lee, C. More than Energy Harvesting − Combining Triboelectric Nanogenerator and Flexible Electronics Technology for Enabling Novel Micro-/Nano-Systems. *Nano Energy* **2019**, *57*, 851−871.

(2) Zhu, G.; Peng, B.; Chen, J.; Jing, Q.; Lin Wang, Z. Triboelectric Nanogenerators as a New Energy Technology: From Fundamentals, Devices, to Applications. *Nano Energy* **2015**, *14*, 126−138.

(3) Dudem, B.; Huynh, N. D.; Kim, W.; Kim, D. H.; Hwang, H. J.; Choi, D.; Yu, J. S. Nanopillar-Array Architectured PDMS-Based Triboelectric Nanogenerator Integrated with a Windmill Model for Effective Wind Energy Harvesting. *Nano Energy* **2017**, *42*, 269−281.

(4) Biswas, P.; Hoque, N. A.; Thakur, P.; Saikh, M. M.; Roy, S.; Khatun, F.; Bagchi, B.; Das, S. Highly Efficient and Durable Piezoelectric Nanogenerator and Photo-Power Cell Based on CTAB Modified Montmorillonite Incorporated PVDF Film. *ACS Sustainable Chem. Eng.* **2019**, *7*, 4801−4813.

(5) Fan, F. R.; Tian, Z. Q.; Lin Wang, Z. Flexible Triboelectric Generator. *Nano Energy* **2012**, *1*, 328−334.

(6) Li, G. Z.; Wang, G. G.; Ye, D. M.; Zhang, X. W.; Lin, Z. Q.; Zhou, H. L.; Li, F.; Wang, B. L.; Han, J. C. High-Performance Transparent and Flexible Triboelectric Nanogenerators Based on PDMS-PTFE Composite Films. *Adv. Electron. Mater.* **2019**, *5*, No. 1800846.

(7) Jiang, Q.; Chen, B.; Yang, Y. Wind-Driven Triboelectric Nanogenerators for Scavenging Biomechanical Energy. *ACS Appl. Energy Mater.* **2018**, *1*, 4269−4276.

(8) Kim, D.; Park, J.; Kim, Y. T. Core-Shell and Helical-Structured Cylindrical Triboelectric Nanogenerator for Wearable Energy Harvesting. *ACS Appl. Energy Mater.* **2019**, *2*, 1357−1362.

(9) Wang, M.; Zhang, J.; Tang, Y.; Li, J.; Zhang, B.; Liang, E.; Mao, Y.; Wang, X. Air-Flow-Driven Triboelectric Nanogenerators for Self-Powered Real-Time Respiratory Monitoring. *ACS Nano* **2018**, *12*, 6156−6162.

(10) Ma, Y.; Zheng, Q.; Liu, Y.; Shi, B.; Xue, X.; Ji, W.; Liu, Z.; Jin, Y.; Zou, Y.; An, Z.; Zhang, W.; Wang, X.; Jiang, W.; Xu, Z.; Wang, Z. L.; Li, Z.; Zhang, H. Self-Powered, One-Stop, and Multifunctional Implantable Triboelectric Active Sensor for Real-Time Biomedical Monitoring. *Nano Lett.* **2016**, *16*, 6042−6051.

(11) Chandrasekhar, A.; Alluri, N. R.; Saravanakumar, B.; Selvarajan, S.; Kim, S. J. Human Interactive Triboelectric Nanogenerator as a Self-Powered Smart Seat. *ACS Appl. Mater. Interfaces* **2016**, *8*, 9692−9699.

(12) Meng, X.; Cheng, Q.; Jiang, X.; Fang, Z.; Chen, X.; Li, S.; Li, C.; Sun, C.; Wang, W.; Wang, Z. L. Triboelectric Nanogenerator as a Highly Sensitive Self-Powered Sensor for Driver Behavior Monitoring. *Nano Energy* **2018**, *51*, 721−727.

(13) Wu, C.; Ding, W.; Liu, R.; Wang, J.; Wang, A. C.; Wang, J.; Li, S.; Zi, Y.; Wang, Z. L. Keystroke Dynamics Enabled Authentication and Identification Using Triboelectric Nanogenerator Array. *Mater. Today* **2018**, *21*, 216−222.

(14) Fan, F. R.; Lin, L.; Zhu, G.; Wu, W.; Zhang, R.; Wang, Z. L. Transparent Triboelectric Nanogenerators and Self-Powered Pressure Sensors Based on Micropatterned Plastic Films. *Nano Lett.* **2012**, *12*, 3109−3114.

(15) Seung, W.; Gupta, M. K.; Lee, K. Y.; Shin, K. S.; Lee, J. H.; Kim, T. Y.; Kim, S.; Lin, J.; Kim, J. H.; Kim, S. W. Nanopatterned Textile-Based Wearable Triboelectric Nanogenerator. *ACS Nano* **2015**, *9*, 3501−3509.

(16) Lee, K. Y.; Chun, J.; Lee, J. H.; Kim, K. N.; Kang, N. R.; Kim, J. Y.; Kim, M. H.; Shin, K. S.; Gupta, M. K.; Baik, J. M.; Kim, S. W. Hydrophobic Sponge Structure-Based Triboelectric Nanogenerator. *Adv. Mater.* **2014**, *26*, 5037−5042.

(17) Chen, J.; Guo, H.; He, X.; Liu, G.; Xi, Y.; Shi, H.; Hu, C. Enhancing Performance of Triboelectric Nanogenerator by Filling High Dielectric Nanoparticles into Sponge PDMS Film. *ACS Appl. Mater. Interfaces* **2016**, *8*, 736−744.

(18) Sriphan, S.; Charoonsuk, T.; Maluangnont, T.; Vittayakorn, N. High-Performance Hybridized Composited-Based Piezoelectric and Triboelectric Nanogenerators Based on BaTiO3/PDMS Composite Film Modified with Ti0.8O2 Nanosheets and Silver Nanopowders Cofillers. *ACS Appl. Energy Mater.* **2019**, *2*, 3840−3850.

(19) Shi, K.; Huang, X.; Sun, B.; Wu, Z.; He, J.; Jiang, P. Cellulose/$BaTiO_3$ Aerogel Paper Based Flexible Piezoelectric Nanogenerators and the Electric Coupling with Triboelectricity. *Nano Energy* **2019**, *57*, 450−458.

(20) Suo, G.; Yu, Y.; Zhang, Z.; Wang, S.; Zhao, P.; Li, J.; Wang, X. Piezoelectric and Triboelectric Dual Effects in Mechanical-Energy Harvesting Using $BaTiO_3$/Polydimethylsiloxane Composite Film. *ACS Appl. Mater. Interfaces* **2016**, *8*, 34335−34341.

(21) Fang, Z.; Chan, K. H.; Lu, X.; Tan, C. F.; Ho, G. W. Surface Texturing and Dielectric Property Tuning toward Boosting of Triboelectric Nanogenerator Performance. *J. Mater. Chem. A* **2018**, *6*, 52−57.

(22) Wang, G.; Xi, Y.; Xuan, H.; Liu, R.; Chen, X.; Cheng, L. Hybrid Nanogenerators Based on Triboelectrification of a Dielectric Composite Made of Lead-Free $ZnSnO_3$ Nanocubes. *Nano Energy* **2015**, *18*, 28−36.

(23) Wang, Z. L. Triboelectric Nanogenerators as New Energy Technology and Self-Powered Sensors - Principles, Problems and Perspectives. *Faraday Discuss.* **2014**, *176*, 447−458.

(24) Jang, S.; Oh, J. H. Rapid Fabrication of Microporous $BaTiO_3$/PDMS Nanocomposites for Triboelectric Nanogenerators through One-Step Microwave Irradiation. *Sci. Rep.* **2018**, *8*, No. 14287.

(25) Menge, H. G.; Kim, J. O.; Park, Y. T. Enhanced Triboelectric Performance of Modified PDMS Nanocomposite Multilayered Nanogenerators. *Materials* **2020**, *13*, No. 4156.

(26) Tantraviwat, D.; Buarin, P.; Suntalelat, S.; Sripumkhai, W.; Pattamang, P.; Rujijanagul, G.; Inceesungvorn, B. Highly Dispersed Porous Polydimethylsiloxane for Boosting Power-Generating Perform-

ance of Triboelectric Nanogenerators. *Nano Energy* **2020**, *67*, No. 104214.
(27) Lee, T. W.; Mitrofanov, O.; Hsu, J. W. P. Pattern-Transfer Fidelity in Soft Lithography: The Role of Pattern Density and Aspect Ratio. *Adv. Funct. Mater.* **2005**, *15*, 1683−1688.
(28) Dudem, B.; Ko, Y. H.; Leem, J. W.; Lee, S. H.; Yu, J. S. Highly Transparent and Flexible Triboelectric Nanogenerators with Sub-wavelength-Architectured Polydimethylsiloxane by a Nanoporous Anodic Aluminum Oxide Template. *ACS Appl. Mater. Interfaces* **2015**, *7*, 20520−20529.
(29) Chergui, N.; Lateb, M.; Lacroix, É; Dufresne, L. CFD Study of Flow Dynamics in a Blade Free Planetary Mixer (BFPM) − a Qualitative Flow Study. *Chem. Eng. Res. Des.* **2015**, *102*, 100−115.
(30) Yamagata, T.; Fujisawa, N. Effect of Rotation and Revolution on Performance of Blade-Free Planetary Mixer. *J. Flow Control, Meas. Visualization* **2019**, *07*, 1−10.
(31) Chun, J.; Kim, J. W.; Jung, W. S.; Kang, C. Y.; Kim, S. W.; Wang, Z. L.; Baik, J. M. Mesoporous Pores Impregnated with Au Nanoparticles as Effective Dielectrics for Enhancing Triboelectric Nanogenerator Performance in Harsh Environments. *Energy Environ. Sci.* **2015**, *8*, 3006−3012.
(32) Lee, J. W.; Cho, H. J.; Chun, J.; Kim, K. N.; Kim, S.; Ahn, C. W.; Kim, I. W.; Kim, J. Y.; Kim, S. W.; Yang, C.; Baik, J. M. Robust Nanogenerators Based on Graft Copolymers via Control of Dielectrics for Remarkable Output Power Enhancement. *Sci. Adv.* **2017**, *3*, No. e1602902.
(33) Niu, S.; Wang, S.; Lin, L.; Liu, Y.; Zhou, Y. S.; Hu, Y.; Wang, Z. L. Theoretical Study of Contact-Mode Triboelectric Nanogenerators as an Effective Power Source. *Energy Environ. Sci.* **2013**, *6*, 3576−3583.
(34) Li, G. Z.; Wang, G. G.; Cai, Y. W.; Sun, N.; Li, F.; Zhou, H. L.; Zhao, H. X.; Zhang, X. N.; Han, J. C.; Yang, Y. A High-Performance Transparent and Flexible Triboelectric Nanogenerator Based on Hydrophobic Composite Films. *Nano Energy* **2020**, *75*, No. 104918.
(35) Liu, G.; Chen, Y.; Gong, M.; Liu, X.; Cui, Z. K.; Pei, Q.; Gu, J.; Huang, C.; Zhuang, Q. Enhanced Dielectric Performance of PDMS-Based Three-Phase Percolative Nanocomposite Films Incorporating a High Dielectric Constant Ceramic and Conductive Multi-Walled Carbon Nanotubes. *J. Mater. Chem. C* **2018**, *6*, 10829−10837.
(36) Feng, S.; Zhang, H.; He, D.; Xu, Y.; Zhang, A.; Liu, Y.; Bai, J. Synergistic Effects of $BaTiO_3$/Multiwall Carbon Nanotube as Fillers on the Electrical Performance of Triboelectric Nanogenerator Based on Polydimethylsiloxane Composite Films. *Energy Technol.* **2019**, *7*, No. 1900101.
(37) Seung, W.; Yoon, H. J.; Kim, T. Y.; Ryu, H.; Kim, J.; Lee, J. H.; Lee, J. H.; Kim, S.; Park, Y. K.; Park, Y. J.; Kim, S. W. Boosting Power-Generating Performance of Triboelectric Nanogenerators via Artificial Control of Ferroelectric Polarization and Dielectric Properties. *Adv. Energy Mater.* **2017**, No. 1600988.
(38) Lin, Z. H.; Cheng, G.; Yang, Y.; Zhou, Y. S.; Lee, S.; Wang, Z. L. Triboelectric Nanogenerator as an Active UV Photodetector. *Adv. Funct. Mater.* **2014**, *24*, 2810−2816.
(39) Lapčinskis, L.; Mā Lnieks, K.; Linarts, A.; Blū Ms, J.; Šmits, K. N.; Järvekülg, M.; Knite, M. R.; Šutka, A. Hybrid Tribo-Piezo-Electric Nanogenerator with Unprecedented Performance Based on Ferroelectric Composite Contacting Layers. *ACS Appl. Energy Mater.* **2019**, *2*, 4027−4032.
(40) Wang, S.; Lin, L.; Wang, Z. L. Nanoscale Triboelectric-Effect-Enabled Energy Conversion for Sustainably Powering Portable Electronics. *Nano Lett.* **2012**, *12*, 6339−6346.
(41) Li, J.; Shepelin, N. A.; Sherrell, P. C.; Ellis, A. V. Poly(Dimethylsiloxane) for Triboelectricity: From Mechanisms to Practical Strategies. *Chem. Mater.* **2021**, *33*, 4304−4327.
(42) He, X.; Guo, H.; Yue, X.; Gao, J.; Xi, Y.; Hu, C. Improving Energy Conversion Efficiency for Triboelectric Nanogenerator with Capacitor Structure by Maximizing Surface Charge Density. *Nanoscale* **2015**, *7*, 1896−1903.
(43) Shi, K.; Zou, H.; Sun, B.; Jiang, P.; He, J.; Huang, X. Dielectric Modulated Cellulose Paper/PDMS-Based Triboelectric Nanogenerators for Wireless Transmission and Electropolymerization Applications. *Adv. Funct. Mater.* **2020**, *30*, No. 1904536.
(44) Kang, X.; Pan, C.; Chen, Y.; Pu, X. Boosting Performances of Triboelectric Nanogenerators by Optimizing Dielectric Properties and Thickness of Electrification Layer. *RSC Adv.* **2020**, *10*, 17752−17759.
(45) Wang, W.; Zhang, J.; Zhang, Y.; Chen, F.; Wang, H.; Wu, M.; Li, H.; Zhu, Q.; Zheng, H.; Zhang, R. Remarkably Enhanced Hybrid Piezo/Triboelectric Nanogenerator via Rational Modulation of Piezoelectric and Dielectric Properties for Self-Powered Electronics. *Appl. Phys. Lett.* **2020**, *116*, No. 023901.
(46) Zhang, P.; Zhang, W.; Deng, L.; Zhang, H. A Triboelectric Nanogenerator Based on Temperature-Stable High Dielectric $BaTiO_3$-Based Ceramic Powder for Energy Harvesting. *Nano Energy* **2021**, *87*, No. 106176.
(47) Šutka, A.; Malnieks, K.; Lapčinskis, L.; Kaufelde, P.; Linarts, A.; Berziņa, A.; Zabels, R.; Jurķans, V.; Gorņevs, I.; Blums, J.; Knite, M. The Role of Intermolecular Forces in Contact Electrification on Polymer Surfaces and Triboelectric Nanogenerators. *Energy Environ. Sci.* **2019**, *12*, 2417−2421.
(48) Šutka, A.; Mālnieks, K.; Lapčinskis, L.; Timusk, M.; Kalniņš, K.; Kovaļovs, A.; Bitenieks, J.; Knite, M.; Stevens, D.; Grunlan, J. Contact Electrification between Identical Polymers as the Basis for Triboelectric/Flexoelectric Materials. *Phys. Chem. Chem. Phys.* **2020**, *22*, 13299−13305.
(49) Lapčinskis, L.; Linarts, A.; Mālnieks, K.; Kim, H.; Rubenis, K.; Pudzs, K.; Smits, K.; Kovaļovs, A.; Kalniņš, K.; Tamm, A.; Jeong, C. K.; Šutka, A. Triboelectrification of Nanocomposites Using Identical Polymer Matrixes with Different Concentrations of Nanoparticle Fillers. *J. Mater. Chem. A* **2021**, *9*, 8984−8990.
(50) Park, K. I.; Bae, S. B.; Yang, S. H.; Lee, H. I.; Lee, K.; Lee, S. J. Lead-Free $BaTiO_3$ Nanowires-Based Flexible Nanocomposite Generator. *Nanoscale* **2014**, *6*, 8962−8968.
(51) Patnam, H.; Dudem, B.; Alluri, N. R.; Mule, A. R.; Graham, S. A.; Kim, S. J.; Yu, J. S. Piezo/Triboelectric Hybrid Nanogenerators Based on Ca-Doped Barium Zirconate Titanate Embedded Composite Polymers for Wearable Electronics. *Compos. Sci. Technol.* **2020**, *188*, No. 107963.
(52) Šutka, A.; Sherrell, P. C.; Shepelin, N. A.; Lapčinskis, L.; Mālnieks, K.; Ellis, A. V. Measuring Piezoelectric Output—Fact or Friction? *Adv. Mater.* **2020**, *32*, No. 2002979.

https://doi.org/10.1021/acsomega.1c04222
ACS Omega 2021, 6, 29765−29773